



Analysis of Mesh Resolution Effect to Numerical Result of CFD-ROM: Turbulent Flow in Stationary Parallel Plate

Candra Damis Widiawaty^{1,2}, Ahmad Indra Siswantara^{1*}, Muhammad Arif Budiyanto¹, Mohammad Arif Andira³, Dendy Adanta⁴, Muhammad Hilman Gumelar Syafe'i^{1,5}, Tanwir Ahmad Farhan¹, Illa Rizianiza^{1,6}

¹ Department of Mechanical Engineering, Faculty of Engineering, Universitas Indonesia, Kampus UI Depok, Depok 16424, Indonesia

² Department of Mechanical Engineering, Politeknik Negeri Jakarta, Depok 16424, Indonesia

³ Air Research Group, Depok, Indonesia

⁴ Department of Mechanical Engineering, Faculty of Engineering, Universitas Sriwijaya, Ogan Ilir-30662, South Sumatera, Indonesia

⁵ Mechanical Engineering, Universitas Negeri Semarang, Semarang 50229, Jawa Tengah, Indonesia

⁶ Mechanical Engineering, Institut Teknologi Kalimantan, Karangjoang Kalimantan Timur 76127, Indonesia

ARTICLE INFO

Article history:

Received 10 October 2023

Received in revised form 12 November 2023

Accepted 11 December 2023

Available online 31 March 2024

Keywords:

CFD-ROM; Mesh Resolution; Turbulent

ABSTRACT

Computational fluid dynamics (CFD) is extensively utilized to predict flow behaviour in various industries and applications. The Full Order Model (FOM) is a high-accuracy approach to flow modelling, but it requires significant computational resources due to its high order and thousands of variables. To address this problem, the Reduced Order Model (ROM) was developed. Despite the advancement brought by ROM, there is a notable gap in research concerning the impact of mesh configuration on CFD-ROM results. While the number of modes has been extensively studied for its influence on CFD-ROM, the mesh configuration, a critical aspect of the simulation process, has received relatively limited attention. This study investigates the effect of mesh resolution on numerical results in CFD-ROM concerning turbulent flow within stationary parallel plates. Employing rigorous methods, including Richardson Extrapolation, verification, validation, and error percentage. The results explicitly confirm that mesh resolution directly impacts the numerical results of the velocity field in CFD-ROM. It is found that there is a notable reduction in Convergence Grid Index (CGI) values for different mesh ratios: 6.401% for medium-to-coarse and 2.031% for fine-to-medium ratio. Thus, with the same mode number, mesh resolution selection can enhance the numerical result of the velocity field in CFD-ROM.

1. Introduction

Computational Fluid Dynamics (CFD) employs sophisticated algorithms to predict various fluid phenomena, making it a vital tool for analyzing fluid flows, including turbulence, heat transfer, particle dispersion, phase changes, and chemical reactions [1-4]. Researchers and practitioners extensively utilize CFD to optimize equipment performance, investigate failures, and improve operational parameters [5-8].

* Corresponding author.

E-mail address: a_indra@eng.ui.ac.id (Ahmad Indra Siswantara)

<https://doi.org/10.37934/cfdl.16.8.117>

The core principle of CFD involves discretizing the continuum equation in both space and time, transforming nonlinear high-order Partial Differential Equations (PDEs) into linear algebraic equations. These equations are organized into a matrix, and computational algorithms like Simple, Simplec, and PISO are used to couple pressure and velocity, determining momentum values in each mesh [9, 10].

Physical flow is considered when determining the mathematical model to be solved. For example, in cavity flow, the prediction of velocity and pressure is computed by solving the equations of conservation of mass and momentum [11]. On the other hand, the temperature and composition of flue gas in the burning of sugarcane bagasse are computed by solving equations of mass conservation, momentum, energy, turbulence, species transportation, and chemical reactions [12]. Therefore, CFD-FOM requires high-order mathematical models and refined mesh to simulate complex flow phenomena [13]. It increased computing time and data storage requirements [14-16].

Based on the previous discussion, CFD-ROM can be used to overcome the limitations of CFD-FOM. CFD-ROM predicts flow phenomena from a reduced mathematical model, which is used initial data from the CFD-FOM simulation results [17-19]. Therefore, it is essential to ensure that the CFD-FOM results are accurate and stable before constructing a reliably reduced model. As command, mesh is one of foundation of numerical in CFD-FOM. Mesh resolution plays a crucial role in CFD, directly impacting result accuracy [20]. Jun Zhang *et al.*, [21] analyzed the effect of mesh resolution, turbulence model, and near-wall models on erosion prediction and found that they affect accuracy. Shan Wang *et al.*, [22] investigated the number and distribution of mesh and width of the water domain for increasing the accuracy of total slamming force, using open Foam. The mesh size also influences the pressure field in the air-particle flow [23]. A mesh independency test is required to obtain verified mesh, which consumes 50% of the simulation work [24].

Based on the principal frame work of CFD-ROM, the accuracy and robustness of CFD-ROM have been trending topics to study. Some researchers have been analyzed the accuracy of CFD-ROM results. In the fluid-thermal back step, it was found that 15 modes had error percentage of 1.02% while the 30 modes had 0.66% [25]. B. Sanderse *et al.*, [26] have analyzed the turbulence on lid cavity-driven flow. It found that 20 modes obtained the highest accuracy of velocity and pressure distribution.

It appears that many studies have focused on enhancing the quality of CFD-ROM simulation result by increasing the number of modes, but little attention to change the mesh resolution. Therefore, this study aims to analyze the impact of mesh resolution on the quality of CFD-ROM results in turbulent flow between two parallel stationary plates. There are 3 different mesh resolutions, denoted as coarse, medium, and fine. The analysis used some method Grid Convergence Index (GCI) using Richardson Extrapolation, alongside verification, validation, and percentage error.

2. Methodology

2.1 Numerical of CFD-FOM

The control volume method discretizes the fluid continuum into elements that have closed surface dS at a fixed control volume Ω [9]. It can be seen in Figure 1.

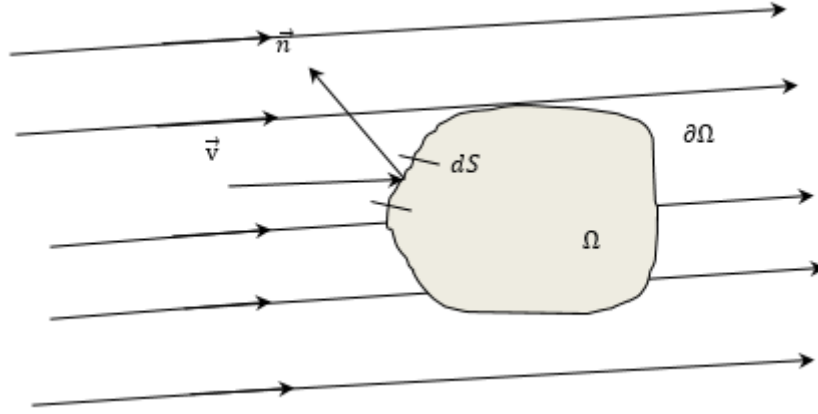


Fig. 1. Finite volume principle in fixed space[9]

The Navier-stokes model is governed by the conservation law and Newton's second law, which predict changes in mass, momentum, and energy within a boundary of control volume [27, 28]. The Navier-Stoke conservation equation are taken from reference [28]:

Mass conservation

$$\partial_t \rho + \text{div}(\rho v) = 0 \quad (1)$$

Momentum conservation

$$\partial_t(\rho v) + \text{div}(\rho v \otimes v) = \text{div} \sigma \quad (2)$$

Energy conservation

$$\partial_t(\rho E) + \text{div}(\rho v H) = \text{div}(\tau v) - \text{div} q \quad (3)$$

$\partial_t \rho$ is the time rate changes of the quantity ρ ($\partial_t \rho = \frac{\partial \rho}{\partial t} + \frac{\partial \rho}{\partial x} + \frac{\partial \rho}{\partial y} + \frac{\partial \rho}{\partial z}$), div is divergence $\text{div}(\rho v) = \frac{\partial \rho u}{\partial x} + \frac{\partial \rho v}{\partial y} + \frac{\partial \rho w}{\partial z}$, u field flow in x ; v in y , w in z direction, \otimes dyadic tensor, σ total surface of stress tensor, E energy, H enthalpy, τ viscous stress tensor, and q heat flux vector.

The Navier-Stokes form in integral and differential is taken from reference [9]:

$$\frac{\partial}{\partial t} \int_{\Omega} \bar{U} \, d\Omega + \int_{\Omega} \nabla \cdot (\bar{F}_c - \bar{F}_v) \, d\Omega = \int_{\Omega} \bar{Q} \, d\Omega \quad (4)$$

$$\frac{\partial \bar{U}}{\partial t} + \nabla \cdot (\bar{F}_c - \bar{F}_v) = \bar{Q} \quad (5)$$

The Math Models of Navier-Stokes is presented below [28] :

$$\frac{\partial \bar{U}}{\partial t} + \frac{\partial \bar{F}}{\partial x} + \frac{\partial \bar{G}}{\partial y} + \frac{\partial \bar{H}}{\partial z} = 0 \quad (6)$$

\vec{U} is conservative variable, \vec{F}_c and \vec{F}_v , convective and viscous flux tensor, \vec{Q} source term, function of $(\vec{F}_c - \vec{F}_v + q)$ in i direction is F ; in j direction G; in k direction H. $\vec{U}, \vec{F}_c, \vec{F}_v, \vec{F}, \vec{G}, \vec{H}, \vec{Q}$ is described as function in Matrix form, can be seen in Table 1:

Table 1

Navier-Stokes equation for 3D

Conservative variable	Sum of convective, viscous, and source term	Viscous stress tensor
$U = \begin{bmatrix} \rho \\ \rho u \\ \rho v \\ \rho w \\ \rho E \end{bmatrix}$	$\vec{F} = \begin{bmatrix} \rho u \\ \rho u^2 + p - \tau_{xx} \\ \rho uv - \tau_{xy} \\ \rho vw - \tau_{xz} \\ \rho uH - \tau_{xx}u - \tau_{xy}v - \tau_{xz}w + q_x \end{bmatrix}$	$\tau_{xx} = 2\mu \frac{\partial u}{\partial x} + \lambda \left(\frac{\partial u}{\partial x} + \frac{\partial v}{\partial y} + \frac{\partial w}{\partial z} \right)$ $\tau_{yy} = 2\mu \frac{\partial v}{\partial y} + \lambda \left(\frac{\partial u}{\partial x} + \frac{\partial v}{\partial y} + \frac{\partial w}{\partial z} \right)$ $\tau_{zz} = 2\mu \frac{\partial w}{\partial z} + \lambda \left(\frac{\partial u}{\partial x} + \frac{\partial v}{\partial y} + \frac{\partial w}{\partial z} \right)$
	$\vec{G} = \begin{bmatrix} \rho u \\ \rho uv - \tau_{yx} \\ \rho u^2 + p - \tau_{yy} \\ \rho vw - \tau_{yz} \\ \rho vH - \tau_{yx}u - \tau_{yy}v - \tau_{yz}w + q_y \end{bmatrix}$	$\tau_{xy} = \tau_{yx} = \mu \left(\frac{\partial u}{\partial y} + \frac{\partial v}{\partial x} \right)$ $\tau_{xz} = \tau_{zx} = \mu \left(\frac{\partial w}{\partial x} + \frac{\partial u}{\partial z} \right)$ $\tau_{xy} = \tau_{yx} = \mu \left(\frac{\partial v}{\partial z} + \frac{\partial w}{\partial y} \right)$
	$\vec{H} = \begin{bmatrix} \rho w \\ \rho uv - \tau_{xx} \\ \rho vw - \tau_{zy} \\ \rho w^2 + p - \tau_{zz} \\ \rho wH - \tau_{zx}u - \tau_{zy}v - \tau_{zz}w + q_z \end{bmatrix}$	

The Standard k-ε model, introduced by Launder and Spalding [29] is a semi-empirical model that assumes fully turbulent flow and neglects the influence of molecular viscosity. It formulates the turbulent kinetic energy equation and turbulence kinetic energy dissipation rate equation as follows:

$$\frac{\partial(\rho k)}{\partial t} + \frac{\partial(\rho k \bar{u}_i)}{\partial x_i} = \frac{\partial}{\partial x_j} \left[\frac{\mu_t}{\sigma_k} \frac{\partial k}{\partial x_j} \right] + 2\mu_t S_{ij} S_{ij} - \rho \varepsilon \quad (7)$$

$$\frac{\partial(\rho \varepsilon)}{\partial t} + \frac{\partial(\rho \varepsilon \bar{u}_i)}{\partial x_i} = \frac{\partial}{\partial x_j} \left[\frac{\mu_t}{\sigma_\varepsilon} \frac{\partial \varepsilon}{\partial x_j} \right] + C_{1\varepsilon} \frac{\varepsilon}{k} 2\mu_t S_{ij} S_{ij} - C_{2\varepsilon} \rho \frac{\varepsilon^2}{k} \quad (8)$$

The equation involves variables such as \bar{u}_i is mean velocity components, S_{ij} is deformation rate or mean velocity gradients, k is turbulent energy, ε turbulent dissipation, and μ_t turbulent viscosity and σ_k is turbulent Prandtl numbers for k and σ_ε is turbulent Prandtl numbers for ε. The default values for all constants have been derived from experimental data for different turbulent flows and are defined as follows: $c_\mu = 0.09$, $c_{1\varepsilon} = 1.44$, $c_{2\varepsilon} = 1.92$, $\sigma_k = 1$, and $\sigma_\varepsilon = 1.3$.

2.2 Numerical of CFD-ROM

The concept of CFD-ROM is to reduce the order of the mathematical model [18]. There are several methods, and POD is one of the prestigious methods for reconstructing ROM, especially for the nonlinear case [17]. Basically, the CFD-ROM solved by offline and online stage [30]. The offline stage consists of discretization, computation of the full-order model, and snapshot for reconstructing the POD bases, while the online stage simulates the fluid flow using the reduced model. The snapshot

process arranges data from the CFD-FOM in matrix form. Therefore, the online stage runs faster than the offline stage because it has a lower order [31].

The POD variable is determined by fluid flow parameters such as velocity (ϕ_i), mass flux(ψ_i), and pressure (χ_i). The mathematical formula for the CFD-ROM is shown below [32]. The matrix formulation of velocity (S_u) and pressure (S_p) is as follows:

$$S_u = [u(\mu^1, t^1), \dots, u(\mu^{N_r}, t^{N_t})] \in \mathbb{R}^{N_u^h \times N_s} \quad (9)$$

$$S_p = [p(\mu^1, t^1), \dots, p(\mu^{N_r}, t^{N_t})] \in \mathbb{R}^{N_p^h \times N_s} \quad (10)$$

The formulation consists of $u(\mu^1, t^1)$ are data points of velocity. μ is parameter space and t is parameter time. N_r is the total number of different parameter set μ . N_t is the total number of time instances or time step. N_u^h represents the number of spatial degrees of freedom (or spatial nodes) in discretization used in CFD. N_s is the total number of snapshots. $p(\mu^1, t^1)$ are data point of pressure.

Generated reduce basis space

$$EN_{POD} = \sum_{i=1}^{N_s} \|u_i - \sum_{k=1}^{N_{POD}} a_k^i \phi_k\| \forall N_{POD} = 1, \dots, N \quad (11)$$

$$(\phi_i, \phi_j)_{L_2(\Omega)} = \delta_{ij} \quad \forall i, j = 1, \dots, N_s \quad (12)$$

$$C^u Q^u = Q^u \lambda^u \quad (13)$$

$$C_{ij}^u = (u_i, u_j)_{L_2(\Omega)} \text{ for } i, j = 1, \dots, N_s \quad (14)$$

EN_{POD} represent due to the error of POD. N_{POD} ranges from 1 to N , which is relates to the modes number. (i, j, k) is vector position. ϕ_i, ϕ_j are basis functions. $L_2(\Omega)$ represents the space of square-integrable functions over the domain. δ_{ij} is the Kronecker delta, which equals 1 when $i=j$ and 0 otherwise. C^u is a correlation matrix, Q^u is a square matrix of eigenvectors, and λ^u is a vector of eigenvalue.

Obtained basis function

$$\phi_i = \frac{1}{N_s \lambda_i^u} \sum_{j=1}^{N_s} u_j Q_{ij}^u \quad (15)$$

Built POD space

$$L_u = [\phi_1, \dots, \phi_{N_u^r}] \in \mathbb{R}^{N_u^h \times N_u^r} \quad (16)$$

$$L_p = [\chi_1, \dots, \chi_{N_p^r}] \in \mathbb{R}^{N_p^h \times N_p^r} \quad (17)$$

λ_i^u represented the eigenvalue associated with the modes. $[\phi_1, \dots, \phi_{N_u^r}]$ represent a set of basic functions or modes. N_u^r represents the number of basic function of velocity. N_p^r represent the number of basic function of pressure. L_u is a matrix u of size $N_u^h \times N_u^r$. L_p is a matrix p of size $N_p^h \times N_p^r$.

Formulated reduced of velocity and pressure

$$u^r \approx \sum_{i=1}^{N_u^r} a_i(t, \mu) \varphi_i(x) \quad (18)$$

$$p^r \approx \sum_{i=1}^{N_p^r} b_i(t, \mu) \chi_i(x) \quad (19)$$

u^r represents a reduced order approximation of velocity. $a_i(t, \mu)$ represents the time and parameter-dependent coefficients associated with each basis function $\varphi_i(x)$. p^r represents a reduced order approximation of pressure. $b_i(t, \mu)$ represents the time and parameter-dependent coefficients associated with each basis function $\chi_i(x)$.

Found coefficient of a_i and b_i

$$M_r \dot{a} - v A_r a + C_r(a) a + B_r b = 0 \quad (20)$$

$$P_r a = 0 \quad (21)$$

Evaluated the a_i and b_i

$$M_{rij} = (\varphi_i, \varphi_j)_{L_2(\Omega)} \quad (22)$$

$$A_{rij} = (\varphi_i, \nabla \cdot 2 \nabla^s \varphi_j)_{L_2(\Omega)} \quad (23)$$

$$B_{rij} = (\varphi_i, \nabla \chi_j)_{L_2(\Omega)} \quad (24)$$

$$P_{rij} = (\chi_i, \nabla \cdot \varphi_j)_{L_2(\Omega)} \quad (25)$$

Computed the reduced model

$$C_{rijk} = (\varphi_i, \nabla \cdot (\varphi_j \otimes \varphi_k))_{L_2(\Omega)} \quad (26)$$

$$R_{ci}^r = (C_r(a) a)_i = a^T C_{ri} a \quad (27)$$

$M_r \dot{a}$, $A_r a$, $C_r(a)$, and B_r are matrix. a and b are coefficient. R_{ci}^r represent the result of Matrix C_{rijk} . T is transpose of matrix.

2.3 Simulation Procedure

Open Foam is used to simulate CFD-FOM [33]. Ithaca FV is utilized to simulate the CFD-ROM [34]. The CFD procedure consists of three stages: pre-processing, processing, and post-processing [35]. In the pre-processor stage, various tasks are performed, including mesh preparation, defining boundary conditions, specifying fluid properties, flow properties, and selecting the turbulence model. The processing stage involves executing the computational simulation, while the post-processing stage

presents the simulation results graphically using graphs, contours, vectors, and animations. The simulation procedure is shown in Figure 2.

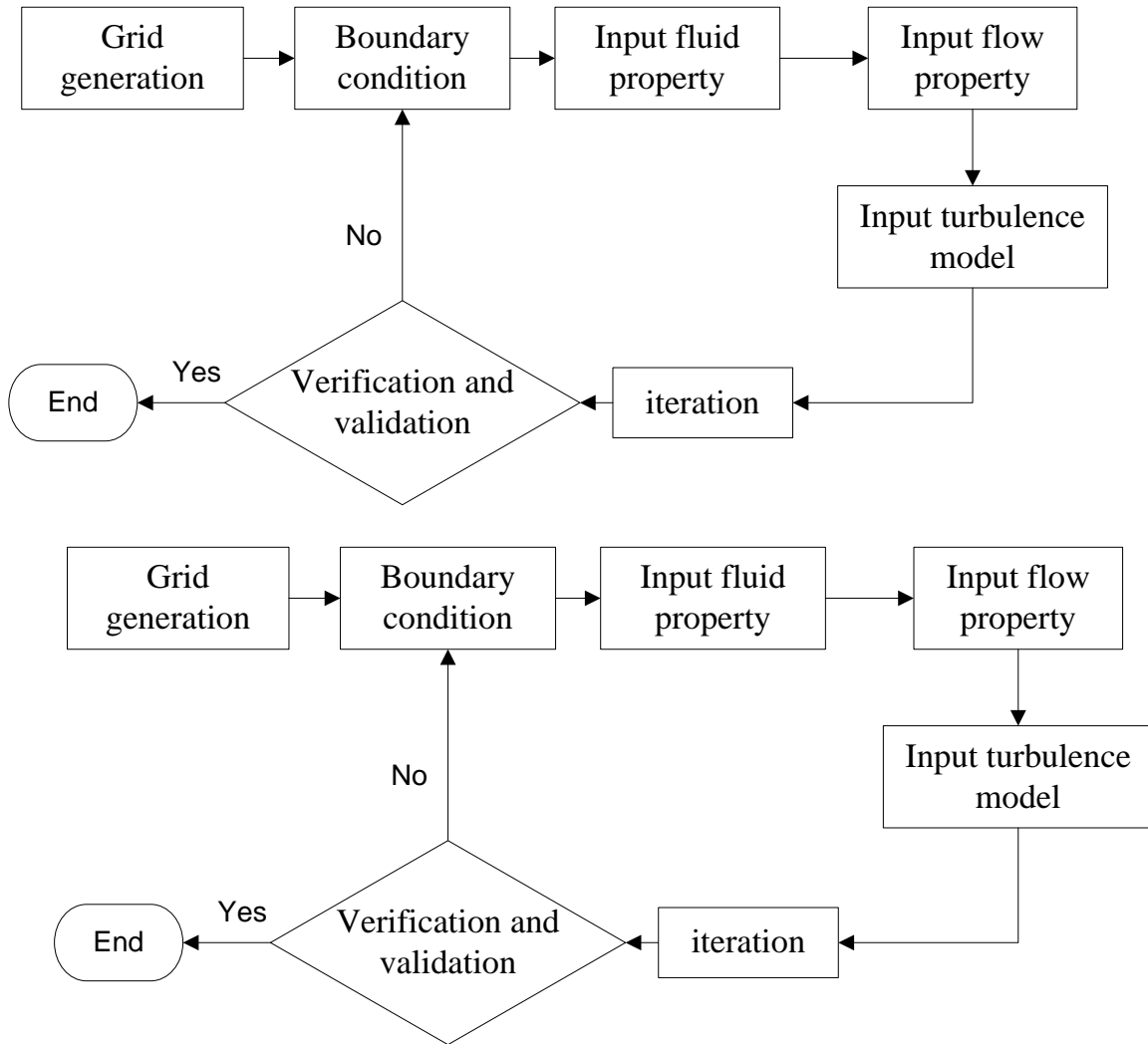


Fig. 2. CFD-FOM procedure

This simulation used air as fluid. Fluid flow is turbulent which used k-epsilon model. Wall set as non-slip wall. The simulation parameter is described in Table 2.

Table 2

Simulation parameter

No	Description	value	Unit
1	Fluid property		
1.1	Density	1.2	kg/m ³
1.2	Dynamic viscosity	0.000005	Pas
2	Flow property		
2.1	Inlet velocity	1	m/s
2.2	k	0.0938	m ² /s ²
2.3	e	1.857	m ² /s ²
3	Turbulence Model	RAS	k-epsilon

The reduced mathematical model is utilized by CFD-ROM to predict the flow, requiring specific simulation procedures. The CFD-ROM simulation procedure is presented in Figure 3. CFD-ROM needs

several inlet velocities to reconstruct the reduced model. This research utilized eighty inlet velocities, as shown in Table 3. The velocity range spans from 0.7 to 1 m/s. CFD-ROM used the same simulation parameters as CFD-FOM. This simulation used 5 modes. However, it's important to note that ITHACA-FV currently employs wall conditions as the default setting.

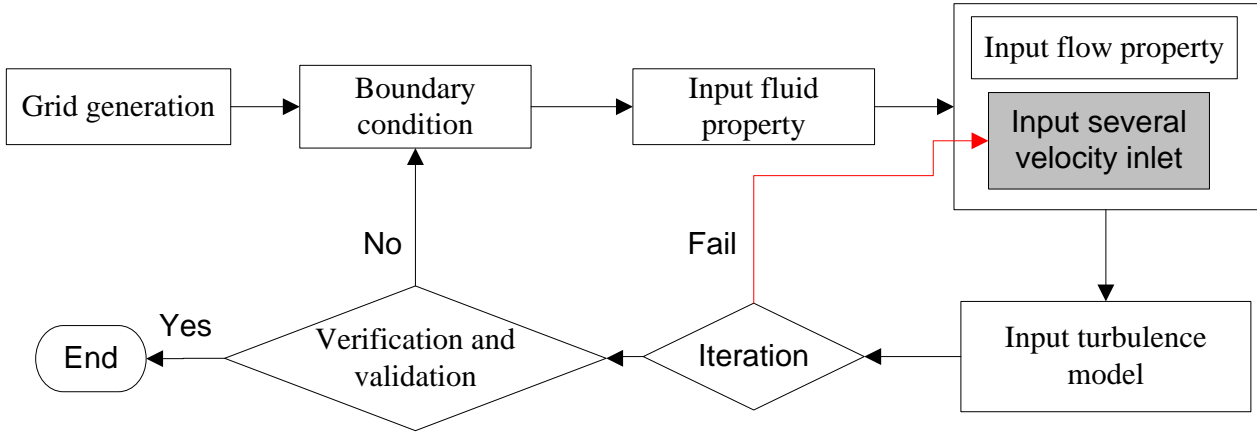


Fig. 3. CFD-ROM procedure

Table 3
 Inlet velocity

Value of Inlet velocity (m/s)							
0.70	0.93	0.86	0.78	0.99	0.92	0.84	0.96
0.71	0.94	0.87	0.80	0.91	0.93	0.86	0.98
0.73	0.96	0.88	0.80	0.92	0.85	0.97	0.98
0.74	0.97	0.90	0.81	0.94	0.86	0.98	0.89
0.76	0.99	0.80	0.82	0.95	0.87	0.98	0.91
0.77	1.00	0.71	0.84	0.96	0.89	1.00	0.82
0.79	1.00	0.73	0.85	0.98	0.89	0.91	0.83
0.90	0.81	0.74	0.87	0.99	0.90	0.92	0.85
1.00	0.83	0.75	0.88	0.99	0.81	0.94	0.86
0.91	0.84	0.77	0.99	0.90	0.83	0.95	0.87

2.4 Geometry and Mesh

The geometry and boundary conditions for the simulation were defined in accordance with the specifications outlined in the referenced source [36]. The geometry's boundaries consist of an inlet, outlet, wall, and symmetry. The length of the plate is 10 m, and the distance between the upper and bottom walls is 0.1 m. The velocity simulation results for CFD-FOM and CFD-ROM were taken at a distance of 2 m from the inlet. The geometry is presented in Figure 4.

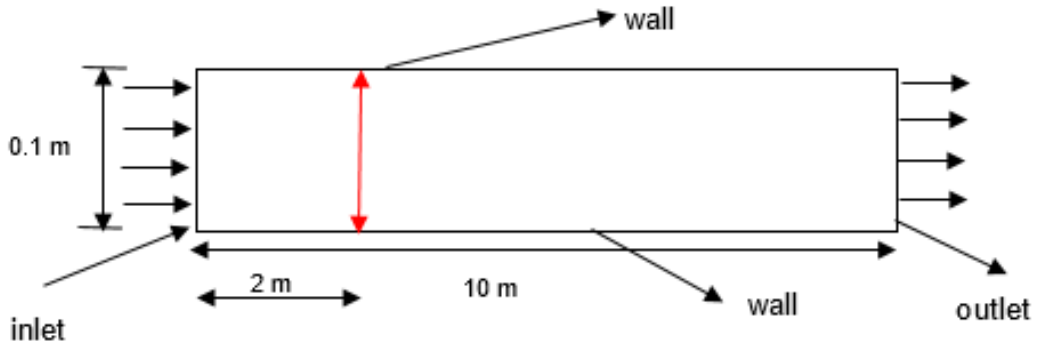


Fig. 4. Geometry [36]

Mesh is generated by using CFDSOF [37]. There are three mesh resolutions, which have different skewness values and aspect ratios. Those parameters affect the mesh quality [38]. This research used three mesh resolutions to analyse the effect of mesh resolution on the CFD-ROM simulation results. The mesh description is shown in Table 4 and mesh resolution is presented in Figure 5.

Table 4

Mesh description

Mesh resolution	Number of mesh	skewness	Max aspect ratio
Coarse	20000	3.622 e-12	8.174
Medium	30000	3.621 e-12	8.286
Fine	70000	1.421 e-12	28

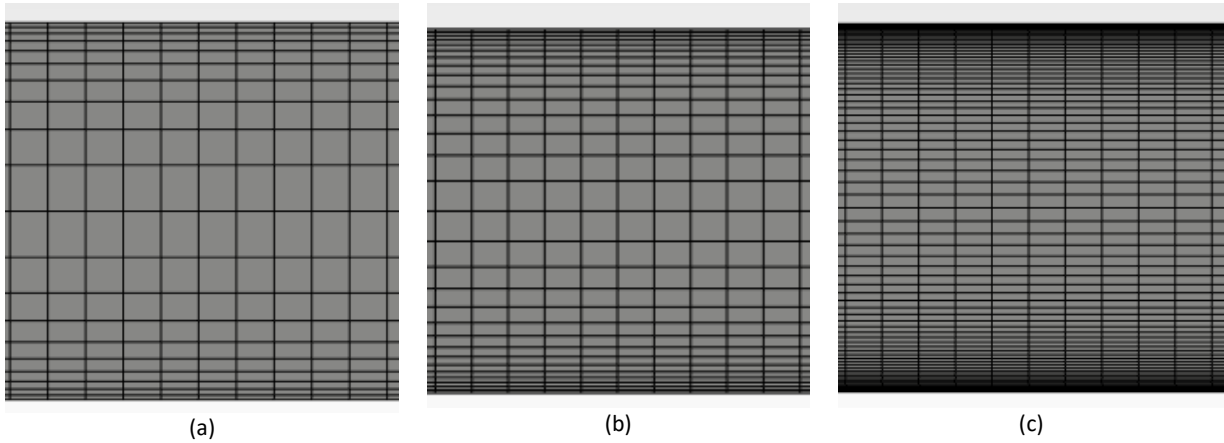


Fig. 5. Mesh resolution

Richardson extrapolation (RE) method is used to predict the discretization error. RE method has been used to select the optimum mesh in CFD-FOM [39]. The equation are as follows [40]:
Calculate mesh size (h)

$$h = \left[\frac{1}{N} \sum_{i=1}^N \Delta A_i \right]^{1/2} \quad (28)$$

$$r_{\text{fine}} = \frac{h_{\text{medium}}}{h_{\text{fine}}} \quad (29)$$

$$r_{\text{medium}} = \frac{h_{\text{coarse}}}{h_{\text{medium}}} \quad (30)$$

r is mesh refinement factor. ΔA_i is the area, and N is the total number of mesh.

Find apparent order (p)

$$p = \frac{1}{\ln(r_{\text{fine}})} \left| \frac{\phi_{\text{coarse}} - \phi_{\text{medium}}}{\phi_{\text{medium}} - \phi_{\text{fine}}} + q(p) \right| \quad (31)$$

$$q(p) = \ln \left(\frac{r_{\text{fine}}^{p-s}}{r_{\text{medium}}^{p-s}} \right) \quad (32)$$

$$s = 1. \text{sign} \left(\frac{\phi_{\text{coarse}} - \phi_{\text{medium}}}{\phi_{\text{medium}} - \phi_{\text{fine}}} \right) \quad (33)$$

Approximate relative error

$$e_a^{\text{medium}} = \left| \frac{(\phi_{\text{medium}} - \phi_{\text{coarse}})}{\phi_{\text{medium}}} \right| \quad (34)$$

$$e_a^{\text{fin}} = \left| \frac{(\phi_{\text{fine}} - \phi_{\text{medium}})}{\phi_{\text{fine}}} \right| \quad (35)$$

e_a^{medium} is relative error of medium to coarse mesh. e_a^{fin} is relative error of fine to medium coarse.

Calculate Grid Convergence Index (GCI)

$$GCI_{\text{medium}} = \frac{1.25 e_a^{\text{medium}}}{r_{\text{medium}}^{p-1}} \quad (36)$$

$$GCI_{\text{fine}} = \frac{1.25 e_a^{\text{fine}}}{r_{\text{fine}}^{p-1}} \quad (37)$$

3. Results

Turbulence flow between two plates is simulated using CFD-FOM and CFD-ROM. Both simulation results are compared with validation data from reference [36]. The plate geometry and the boundaries are shown in Figure 1. All simulations are run on a normal desktop with an Intel Core i7 processor at 3.2 GHz and 8 GB of RAM. Three meshes with different resolutions are chosen: coarse, medium, and fine.

The results of the discretization error analysis using the Richardson Extrapolation method are shown in Table 5. It can be observed that the relative error predictions for the coarse-to-medium and medium-to-fine ratios in CFD-FOM are 1.020% and 0.211%, respectively. In contrast, the relative error predictions in CFD-ROM are 3.643% and 3.339%, respectively. It indicates that the CFD-FOM and CFD-ROM simulation methods have different predictions for the maximum velocity for the same mesh resolution. Nevertheless, there the error reduced when used fine mesh resolution both CFD-FOM and CFD-ROM.

Table 5
 Calculation of discretization error based on maximum velocity

Description	CFD-FOM	CFD-ROM	Unit	Note
h_{coarse}	0.00333		m	
h_{medium}	0.00222		m	
h_{fine}	0.000952		m	
r_{medium}	1.500			
r_{fine}	2.333			
ϕ_{coarse}	1.198	1.230	m/s	$x = 2 \text{ m}; y = 0.05 \text{ m}$
ϕ_{medium}	1.186	1.277	m/s	$x = 2 \text{ m}; y = 0.05 \text{ m}$
ϕ_{fine}	1.184	1.342	m/s	$x = 2 \text{ m}; y = 0.05 \text{ m}$
p	4.298	1.32		
ea_{medium}	1.020	3.643	%	
ea_{fine}	0.211	3.339	%	
GCI _{medium}	0.271	6.401	%	
GCI _{fine}	0.0071	2.013	%	

Figure 6 presents a comparison of the monotonic convergence graph results from CFD-FOM and CFD-ROM. The results show that CFD-FOM predicted the maximum velocity for coarse, medium, and fine meshes as 1.198 m/s, 1.186 m/s, and 1.184 m/s, respectively. Conversely, the CFD-ROM method approximated the maximum velocity for each mesh resolution at 1.230 m/s, 1.277 m/s, and 1.340 m/s, respectively. Both CFD methods show convergence in the numerical results. Furthermore, the results indicate that the finer mesh can significantly reduce the discretization error for CFD-FOM more than for CFD-ROM. Thus, mesh resolution influences the numerical results of both CFD methods.

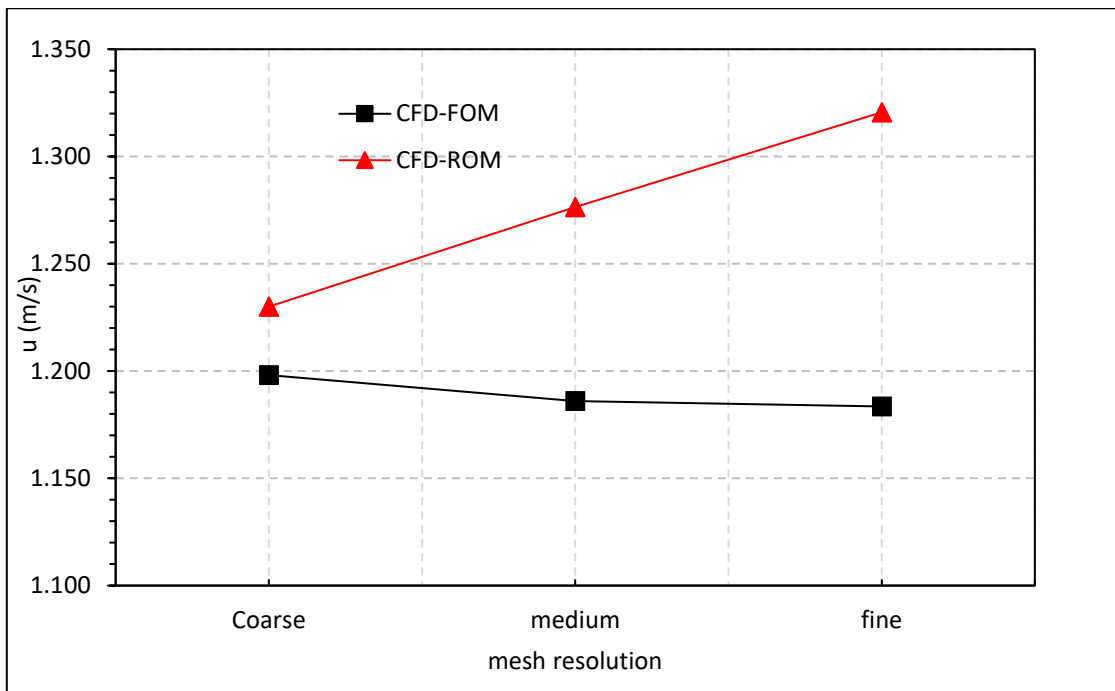


Fig. 6. Monotonic convergence graph

After the discretization error analysis, the simulation results of CFD-FOM were then verified, as shown in Figure 7. It shows the velocity field and velocity vector from the CFD-FOM simulation results. It observes that the low velocity formed near the walls, while the highest velocity formed between the top and bottom plates for all mesh resolution. It is in good agreement with the concept of the

boundary layer in the stationary plate [41]. It found that the refines mesh can predict the lower velocity near the wall.

After the discretization error analysis, the simulation results of CFD-FOM were then verified, as shown in Figure 7. It shows the velocity field and velocity vector from the CFD-FOM simulation results. It observes that the low velocity formed near the walls, while the highest velocity formed between the top and bottom plates for all mesh resolution. It is in good agreement with the concept of the boundary layer in the stationary plate [41]. It found that the refines mesh can predict the lower velocity near the wall.

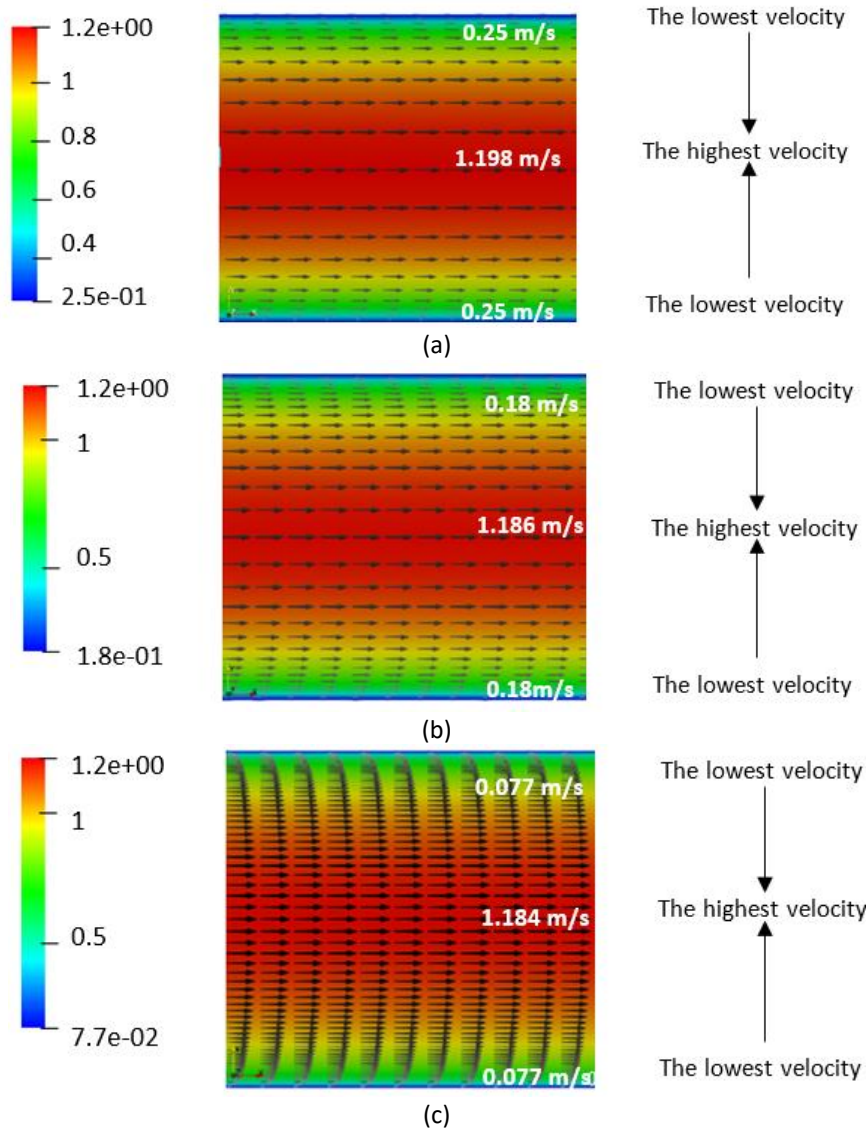


Fig. 7. The simulation result of contour and vector velocity of CFD-FOM (a) coarse mesh (b) medium mesh (c) fine mesh

Thereafter, it compared the results of CFD-FOM to comprehensively analyse mesh resolution as shown in Figure 8. All mesh resolutions exhibit the same curve pattern as the validation data. The curves tend to be flat near the maximum velocity. These velocity yield curves show good agreement with the characteristics of turbulent flow [36]. The results from the three mesh resolutions align with the velocity field predictions in the validation data. Specifically, the fine mesh predicts both the minimum and maximum velocity results in accordance with the validation data.

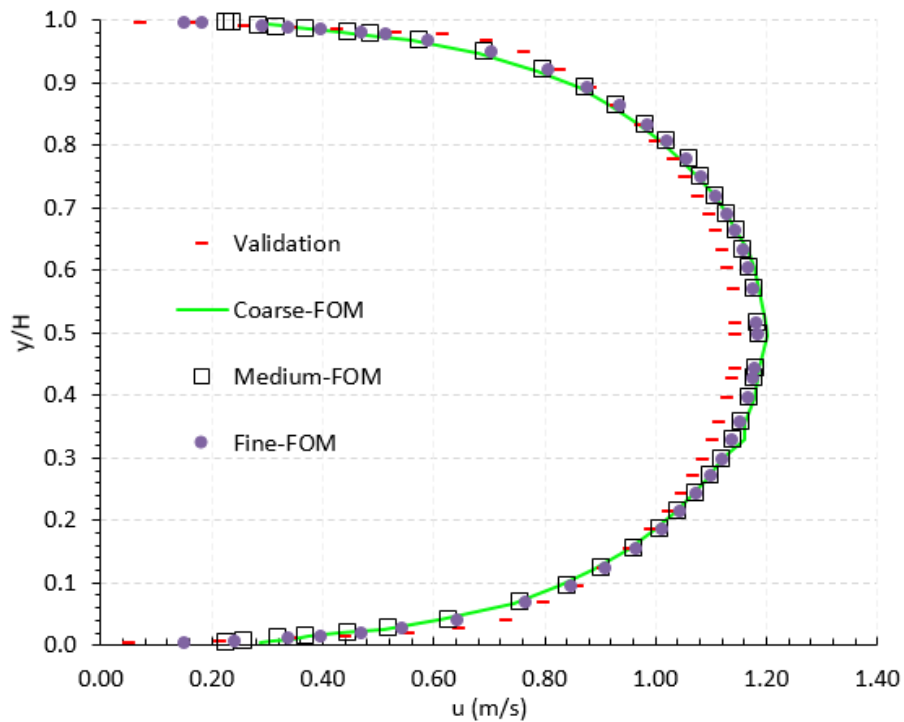
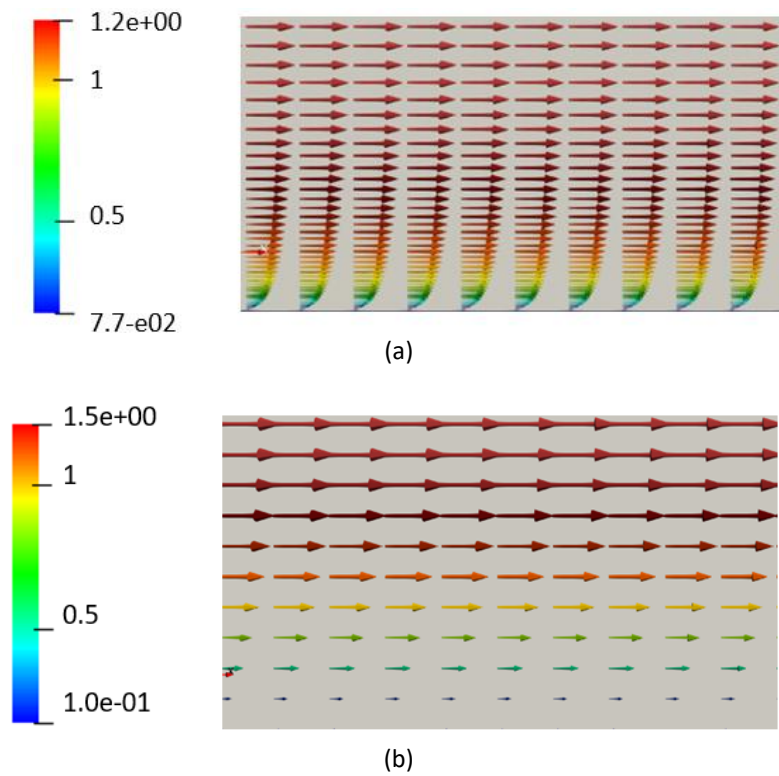


Fig. 8. Velocity field of CFD-FOM result compare to the validation data

Figure 9 represents the comparison of CFD-ROM results for all mesh resolution with CFD-FOM result of fine mesh. Generally, the CFD-ROM results have a good agreement with the CFD-FOM. The finer mesh results of CFD-ROM can predict the lower velocity near the plates. It indicates that the mesh resolution affects the numerical result. Compare to CFD-FOM result for fine mesh, the CFD-ROM can produce the lower velocity near the plate. It implies that the mathematics model influences the numerical result. The velocity yield of CFD-ROM as shown in Figure 9.



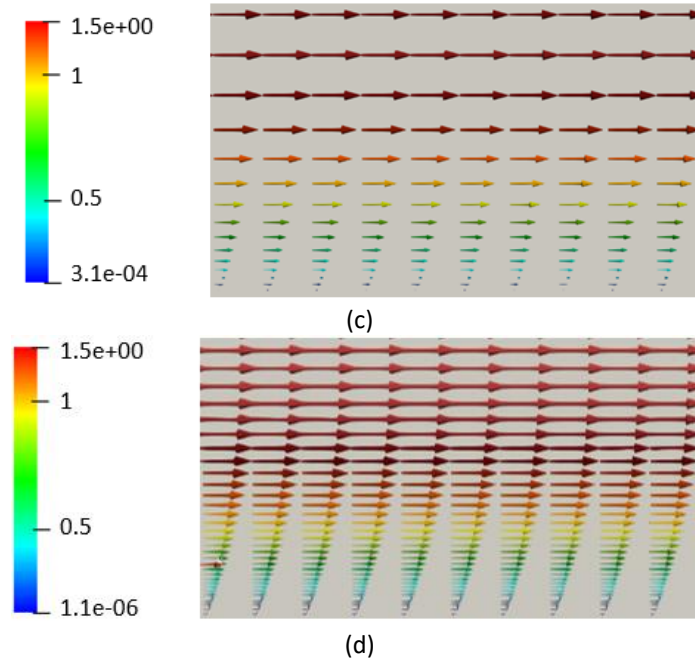


Fig. 9. Velocity vector of CFD-ROM compare to CFD-FOM for fine mesh (a) fine-FOM (b) coarse-ROM (c) medium-ROM (d) fine-ROM

As plotted in Figure 10, the velocity yield of CFD-ROM results varies as the increase in mesh resolution. It shows the CFD-ROM can predict the velocity near the wall close to validation data for all mesh resolutions. Whereas, CFD-ROM over predict the maximum velocity compare to validation data. These range velocity field produce a parabolic curve for all the mesh resolution which is difference from the validation data. It indicates that the velocity near the maximum velocity is more varies compare to validation data. However, refine mesh has a widest curve compare to coarse and medium.

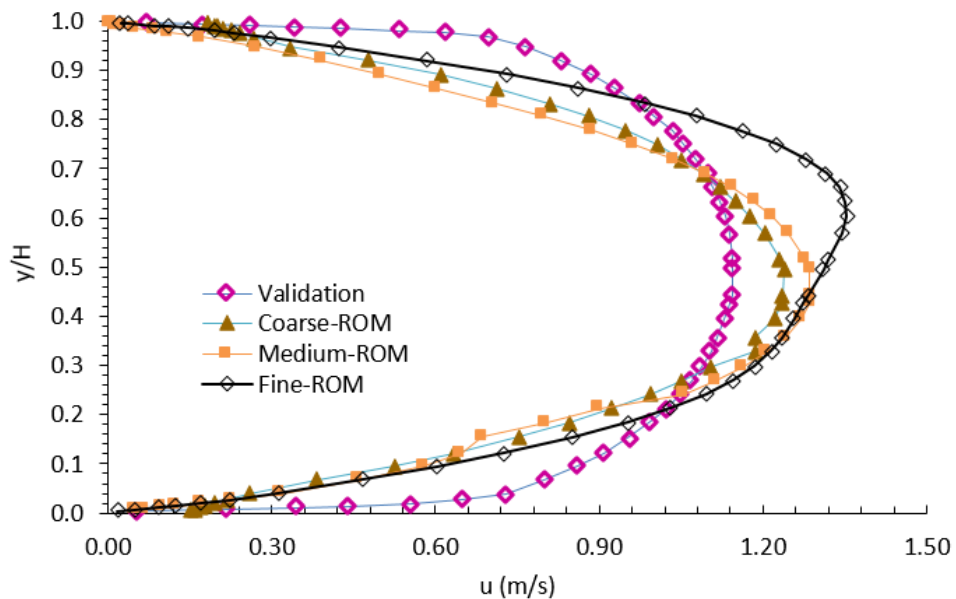


Fig. 10. Velocity yield of CFD ROM compare to validation data

Furthermore, the average velocity simulated by CFD-ROM is compared to validation data. Error percentage is used. R_{coarse} , R_{medium} , and R_{fine} are follow:

$$R_{\text{coarse}} = \left| \frac{|u_{\text{ave}}| - |u_{\text{ave}}^{\text{ROM}}|}{|u_{\text{ave}}|} \right| \quad (38)$$

$$R_{\text{medium}} = \left| \frac{|u_{\text{ave}}| - |u_{\text{ave}}^{\text{ROM}}|}{|u_{\text{ave}}|} \right| \quad (39)$$

$$R_{\text{fine}} = \left| \frac{|u_{\text{ave}}| - |u_{\text{ave}}^{\text{ROM}}|}{|u_{\text{ave}}|} \right| \quad (40)$$

Table 6 represents the error percentage of average velocity. The coarse, medium, and fine mesh has 15.038%, 19.117%, and 7.577%, respectively. The refiner of mesh resolution from coarse to medium, the error percentage is increased. Meanwhile, from medium to fine mesh, the error percentage is decrease. However, the fine mesh gives the lowest error percentage. It indicates that the appropriate mesh resolution can effectively reduce the numerical error in CFD-ROM.

Table 6
Error percentage of CFD-ROM compare to validation data

Description	U_{ave} (m/s)	% error
Validation	0.820	
coarse-ROM	0.697	15.038
medium-ROM	0.663	19.117
fine-ROM	0.758	7.577

4. Conclusions

In this study, we investigated the impact of mesh resolution on velocity field results in CFD-ROM without change the number of modes. It used Richardson extrapolation, verification, validation, and % error percentage methods. Simulations were conducted using the open-source libraries Open Foam for CFD-FOM and ITHACA-FV for CFD-ROM, while Paraview was employed for visualization.

The investigation clearly shows that mesh resolution influences the numerical results in CFD-ROM. The observed decrease in CGI values for coarse-to-medium and medium-to-fine ratios was 6.401% and 2.031% respectively. Verification results affirm that CFD-ROM velocity yield for various mesh resolutions has good agreement with the boundary layer concept. Additionally, it is found variations in numerical results for minimum and maximum velocity. The CFD-ROM velocity field for the three mesh resolutions exhibits a broader velocity range, resulting in a steeper slope of the velocity difference compared to the validation data. The medium mesh produces the highest error of average velocity of validation data, reaching 19.117%, while the fine mesh obtains the lowest error at 7.577%. Hence, selecting an appropriate mesh resolution can enhance the accuracy of the velocity field in CFD-ROM without increasing number of modes, for turbulent flows with a Reynolds number of 12000. However, the result of CFD-FOM by using fine mesh has more nearly to the validation data than the result of CFD-ROM as shown in Figure 8 and Figure 10.

Acknowledgement

This research was funded by a grant from Universitas Indonesia with scheme (PUTI) Pasca Sarjana 2023 and PT. CCIT was facilitated CFDSOF.

References

- [1] Krastev, Vesselin Krassimirov, Luca Silvestri, and Gino Bella. "Effects of turbulence modeling and grid quality on the zonal URANS/LES simulation of static and reciprocating engine-like geometries." *SAE International Journal of Engines* 11, no. 6 (2018): 669-686. <https://doi.org/10.4271/2018-01-0173>
- [2] Xu, Guangping, and Jiasong Wang. "CFD modeling of particle dispersion and deposition coupled with particle dynamical models in a ventilated room." *Atmospheric Environment* 166 (2017): 300-314. <https://doi.org/10.1016/j.atmosenv.2017.07.027>
- [3] Ramdhan, G. Gun Gun, Ahmad Indra Siswantara, Asyari Daryus, and Hariyotejo Pujowidodo. "Turbulence model and validation of air flow in wind tunnel." *International Journal of Technology* 7, no. 8 (2016): 1362-1371. <https://doi.org/10.14716/ijtech.v7i8.6891>
- [4] Siswantara, Ahmad Indra, Budiarmo, and Steven Darmawan. "Investigation of Inverse-Turbulent-Prandtl Number with Four RNG k-ε Turbulence Models on Compressor Discharge Pipe of Bioenergy Micro Gas Turbine." *Applied Mechanics and Materials* 819 (2016): 392-400. <https://doi.org/10.4028/www.scientific.net/AMM.819.392>
- [5] Widiawaty, C. D., A. I. Siswantara, G. G. R. Gunadi, H. Pujowidodo, and M. H. G. Syafei. "A CFD simulation and experimental study: predicting heat transfer performance using SST k-ω turbulence model." In *IOP Conference Series: Materials Science and Engineering*, vol. 909, no. 1, p. 012004. IOP Publishing, 2020. <https://doi.org/10.1088/1757-899X/909/1/012004>
- [6] Widiawaty, Candra Damis, Ahmad Indra Siswantara, Budiarmo Budiarmo, Asyari Daryus, Gun Gun Ramdhan Gunadi, and Hariyotejo Pujowidodo. "Investigation the effect of superficial velocity to the heat transfer in bubbling regime of fluidization using CFD simulation." In *AIP Conference Proceedings*, vol. 2187, no. 1. AIP Publishing, 2019. <https://doi.org/10.1063/1.5138279>
- [7] Wang, Kan, Tingting Shi, Yuru He, Mingzhi Li, and Xinming Qian. "Case analysis and CFD numerical study on gas explosion and damage processing caused by aging urban subsurface pipeline failures." *Engineering Failure Analysis* 97 (2019): 201-219. <https://doi.org/10.1016/j.engfailanal.2019.01.052>
- [8] Khanjanpour, Mohammad Hassan, and Akbar A. Javadi. "Optimization of a Horizontal Axis Tidal (HAT) turbine for powering a Reverse Osmosis (RO) desalination system using Computational Fluid Dynamics (CFD) and Taguchi method." *Energy Conversion and Management* 231 (2021): 113833. <https://doi.org/10.1016/j.enconman.2021.113833>
- [9] Blazek, Jiri. *Computational fluid dynamics: principles and applications*. Butterworth-Heinemann, 2015. <https://doi.org/10.1016/B978-0-08-099995-1.00012-9>
- [10] van Leer, Bram, and Kenneth G. Powell. "Introduction to computational fluid dynamics." *Encyclopedia of Aerospace Engineering* (2010). <https://doi.org/10.1002/9780470686652.eae048>
- [11] Sciacchitano, A., F. Arpino, and G. Cortellessa. "Benchmark PIV database for the validation of CFD simulations in a transitional cavity flow." *International Journal of Heat and Fluid Flow* 90 (2021): 108831. <https://doi.org/10.1016/j.ijheatfluidflow.2021.108831>
- [12] Centeno-González, Felipe Orlando, Electro Eduardo Silva Lora, Helcio Francisco Villa Nova, Lourival Jorge Mendes Neto, Arnaldo Martín Martínez Reyes, Albert Ratner, and Mohsen Ghamari. "CFD modeling of combustion of sugarcane bagasse in an industrial boiler." *Fuel* 193 (2017): 31-38. <https://doi.org/10.1016/j.fuel.2016.11.105>
- [13] Weinman, K. A., M. Fagner, Ralf Deiterding, Daniela Heine, Uwe Fey, F. Braenstroem, B. Schultz, and Claus Wagner. "Assessment of the mesh refinement influence on the computed flow-fields about a model train in comparison with wind tunnel measurements." *Journal of Wind Engineering and Industrial Aerodynamics* 179 (2018): 102-117. <https://doi.org/10.1016/j.jweia.2018.05.005>
- [14] Stabile, Giovanni, Saddam Hijazi, Andrea Mola, Stefano Lorenzi, and Gianluigi Rozza. "POD-Galerkin reduced order methods for CFD using Finite Volume Discretisation: vortex shedding around a circular cylinder." *Communications in Applied and Industrial Mathematics* 8, no. 1 (2017): 210-236. <https://doi.org/10.1515/caim-2017-0011>
- [15] Schilders, Wil. "Introduction to model order reduction." In *Model order reduction: theory, research aspects and applications*, pp. 3-32. Berlin, Heidelberg: Springer Berlin Heidelberg, 2008. https://doi.org/10.1007/978-3-540-78841-6_1
- [16] Gao, Xi, Tingwen Li, William A. Rogers, Kristin Smith, Katherine Gaston, Gavin Wiggins, and James E. Parks II. "Validation and application of a multiphase CFD model for hydrodynamics, temperature field and RTD simulation in a pilot-scale biomass pyrolysis vapor phase upgrading reactor." *Chemical Engineering Journal* 388 (2020): 124279. <https://doi.org/10.1016/j.cej.2020.124279>
- [17] Georgaka, Sokratia, Giovanni Stabile, Kelbij Star, Gianluigi Rozza, and Michael J. Bluck. "A hybrid reduced order method for modelling turbulent heat transfer problems." *Computers & Fluids* 208 (2020): 104615. <https://doi.org/10.1016/j.compfluid.2020.104615>

- [18] Liu, Yang, Wuxuan Pan, and Zhengwei Long. "Optimization of air supply parameters for stratum ventilation based on proper orthogonal decomposition." *Sustainable Cities and Society* 75 (2021): 103291. <https://doi.org/10.1016/j.scs.2021.103291>
- [19] Zimmermann, Ralf. "Gradient-enhanced surrogate modeling based on proper orthogonal decomposition." *Journal of Computational and Applied Mathematics* 237, no. 1 (2013): 403-418. <https://doi.org/10.1016/j.cam.2012.06.010>
- [20] Gullberg, Rebecca. "Computational fluid dynamics in OpenFOAM." *Mesh Generation and Quality*. TKP 4555 (2017).
- [21] Zhang, Jun, Farzin Darihaki, and Siamack A. Shirazi. "A comprehensive CFD-based erosion prediction for sharp bend geometry with examination of grid effect." *Wear* 430 (2019): 191-201. <https://doi.org/10.1016/j.wear.2019.04.029>
- [22] Wang, Shan, Jorge Gadelho, Hafizul Islam, and C. Guedes Soares. "CFD modelling and grid uncertainty analysis of the free-falling water entry of 2D rigid bodies." *Applied Ocean Research* 115 (2021): 102813. <https://doi.org/10.1016/j.apor.2021.102813>
- [23] Shao, Yingjuan, Jinrao Gu, Wenqi Zhong, and Aibing Yu. "Determination of minimum fluidization velocity in fluidized bed at elevated pressures and temperatures using CFD simulations." *Powder Technology* 350 (2019): 81-90. <https://doi.org/10.1016/j.powtec.2019.03.039>
- [24] Slotnick, Jeffrey P., Abdollah Khodadoust, Juan Alonso, David Darmofal, William Gropp, Elizabeth Lurie, and Dimitri J. Mavriplis. *CFD vision 2030 study: a path to revolutionary computational aerosciences*. No. NF1676L-18332. 2014.
- [25] Deep, Dewanshu, Ashwin Sahasranaman, and S. Senthilkumar. "POD analysis of the wake behind a circular cylinder with splitter plate." *European Journal of Mechanics-B/Fluids* 93 (2022): 1-12. <https://doi.org/10.1016/j.euromechflu.2021.12.010>
- [26] Sanderse, Benjamin. "Non-linearly stable reduced-order models for incompressible flow with energy-conserving finite volume methods." *Journal of Computational Physics* 421 (2020): 109736. <https://doi.org/10.1016/j.jcp.2020.109736>
- [27] Hami, Khelifa. "Turbulence Modeling a Review for Different Used Methods." *International Journal of Heat & Technology* 39, no. 1 (2021). <https://doi.org/10.18280/ijht.390125>
- [28] Masatsuka, Katate. *I do Like CFD, vol. 1*. Vol. 1. Lulu. com, 2009.
- [29] Launder, Brian Edward, and Dudley Brian Spalding. "The numerical computation of turbulent flows." In *Numerical prediction of flow, heat transfer, turbulence and combustion*, pp. 96-116. Pergamon, 1983. <https://doi.org/10.1016/B978-0-08-030937-8.50016-7>
- [30] Calzolari, Giovanni, and Wei Liu. "Deep learning to replace, improve, or aid CFD analysis in built environment applications: A review." *Building and Environment* 206 (2021): 108315. <https://doi.org/10.1016/j.buildenv.2021.108315>
- [31] Ballarin, Francesco, Andrea Manzoni, Alfio Quarteroni, and Gianluigi Rozza. *Supremizer stabilization of POD-Galerkin approximation of parametrized Navier-Stokes equations*. MATHICSE Technical Report, École Polytechnique Fédérale de Lausanne, 2014. <https://doi.org/10.1002/nme.4772>
- [32] Stabile, Giovanni, and Gianluigi Rozza. "Finite volume POD-Galerkin stabilised reduced order methods for the parametrised incompressible Navier-Stokes equations." *Computers & Fluids* 173 (2018): 273-284. <https://doi.org/10.1016/j.compfluid.2018.01.035>
- [33] Lande, Anne Marie. "Complex mesh generation with openfoam." Master's thesis, University of South-Eastern Norway, 2021.
- [34] ITHACA-FV, "06POD_RBF.C." [Online]. Available: https://mathlab.github.io/ITHACA-FV/06POD_RBF_8C-example.html.
- [35] Silvestri, Luca. "CFD modeling in Industry 4.0: New perspectives for smart factories." *Procedia Computer Science* 180 (2021): 381-387. <https://doi.org/10.1016/j.procs.2021.01.359>
- [36] Tu, Jiyan, Guan Heng Yeoh, Chaoqun Liu, and Yao Tao. *Computational fluid dynamics: a practical approach*. Elsevier, 2018.
- [37] cfdsof, "No Title." [Online]. Available: <https://cfdsof.com/>.
- [38] Mavriplis, Dimitri J. "Mesh generation and adaptivity for complex geometries and flows." In *Handbook of computational fluid mechanics*, pp. 417-459. Academic Press, 1996. <https://doi.org/10.1016/B978-0-12553010-1/50008-6>
- [39] Widiawaty, Candra Damis, Ahmad Indra Siswantara, Gun Gun R. Gunadi, Mohamad Arif Andira, Muhammad Arif Budiyanto, M. Hilman Gumelar Syafei, and Dendy Adanta. "Optimization of inverse-Prandtl of Dissipation in standard k-ε Turbulence Model for Predicting Flow Field of Crossflow Turbine." *CFD Letters* 14, no. 1 (2022): 112-127. <https://doi.org/10.37934/cfdl.14.1.112127>
- [40] Roache, Patrick J., Kirti N. Ghia, and Frank M. White. "Editorial policy statement on the control of numerical accuracy." *Journal of Fluids Engineering* 108, no. 1 (1986): 2. <https://doi.org/10.1115/1.3242537>
- [41] Yunus, A. Cengel. *Fluid Mechanics: Fundamentals And Applications (Si Units)*. Tata McGraw Hill Education Private Limited, 2010.